Nanoscale

ROYAL SOCIETY OF CHEMISTRY

COMMUNICATION

View Article Online
View Journal | View Issue

Cite this: *Nanoscale*, 2021, **13**, 11793

Received 19th April 2021,
Accepted 7th June 2021

DOI: 10.1039/d1nr02478g

rsc.li/nanoscale

Probing the plasmon-driven Suzuki–Miyaura coupling reactions with cargo-TERS towards tailored catalysis†

Zhandong Li[a] and Dmitry Kurouski *[a,b]

We present a label-free approach that is based on tip-enhanced Raman spectroscopy (TERS) for a direct *in situ* assessment of the molecular reactivity in plasmon-driven reactions. Using this analytical approach, named cargo-TERS, we investigate the relationship between the chemical structure of aromatic halides and the catalytic probability of the Suzuki–Miyaura coupling reaction on gold–palladium bimetallic nanoplates (Au@PdNPs). We demonstrate that cargo-TERS can be used to quantify the yield of biphenyl-4,4′-dithiol (BPDT), the product of the coupling reaction. Our results also show that the halide reactivity decreases from bromo through chloro to fluorohalides. Finally, we employ this novel imaging technique to unravel the nanoscale reactivity and selectivity of Au@PdNPs. We find that the edges and corners of these nanostructures exhibit the highest catalytic reactivity, while the flat terraces of Au@PdNPs remain catalytically inactive.

Introduction

The tailored synthesis of novel drug candidates, polymers, and organic and inorganic catalysts with desired properties requires an extensive understanding of molecular interactions.[1–3] Traditionally, such interactions are examined *via* routine synthetic[2] approaches or by in-silica computational simulations.[4] The former strategy is labor- and reagent-intensive, whereas the latter is often inaccurate because it is extremely difficult to model for all details of molecular interactions. Several analytical techniques, such as infrared spectroscopy[5] and nuclear magnetic resonance (NMR)[6] analysis, can be used to probe molecular interactions and determine the reactivity of molecular species. However, these tools typically require large volumes and high concentrations of analytes. This catalyzed a search for advanced analytical approaches that can unravel molecular interactions in general and the molecular reactivity in particular with femto or attoliters of analytes.

Tip-Enhanced Raman spectroscopy (TERS) is a modern analytical technique that possesses single-molecule sensitivity and sub-nanometer spatial resolution.[7–10] In TERS, localized surface plasmon resonances (LSPRs) are generated by electromagnetic radiation at the apex of a metalized scanning probe.[11,12] Once the probe is brought to the surface of interest, LSPRs will enhance Raman scattering from molecules located directly underneath it up to 10^6–10^8.[13,14] This strong electromagnetic enhancement allows for single molecule detection on analyzed surfaces.[15,16] Next, the probe can be placed above the surface to obtain a chemical image of the sample with Angstrom spatial resolution.[17] This makes TERS a technique of choice in numerous research applications including nucleic acid sequencing,[18,19] amyloid biology,[20–25] polymer and surface science,[26–31] electrochemistry[32–35] and catalysis.[36–42]

Experimental evidence showed that TERS can be used to unravel plasmon-driven processes on mono[41–43] and bimetallic[36–39] nanostructures. These processes are driven by hot carriers, highly energetic species that appear as a result of direct interband, phonon-assisted intraband, and geometry-assisted decays of LSPRs.[44–48] Using TERS and phenyl isocyanide (PIC) as a molecular reporter, Ren's group examined the catalytic properties of the edges of the sub-monolayer of Pd on Au surfaces. The researchers found that the C≡N vibration of PIC at the edges of Pd islands was red-shifted by 60 cm^{-1} relative to the position of this band in the spectra obtained from the molecules located on Pd terraces. It was concluded that Pd edges have higher reactivity relative to Pd atoms on terraces.[49] Similar conclusions were made from the TERS images of the rectified optical fields on the surface of silver nanowires (AgNWs) and silver nanoparticles (AgNPs).[50,51] El-Khoury's group found that the edges of both AgNPs and AgNWs had a higher intensity of the rectified electric field compared to the central part of these plasmonic nanostructures. Our group

[a]*Department of Biochemistry and Biophysics, Texas A&M University, College Station, Texas 77843, USA. E-mail: dkurouski@tamu.edu*
[b]*The Institute for Quantum Science and Engineering, Texas A&M University, College Station, Texas, 77843, USA*

†Electronic supplementary information (ESI) available. See DOI: 10.1039/d1nr02478g

found that gold–palladium microplates (Au@PdMPs) exhibited unique catalytic properties that were not observed in monometallic nanostructures (AuMPs).[36,39] These bimetallic nanostructures are capable of light-driven reduction of 4-NBT to both 4-ATP and DMAB, whereas only DMAB was detected as a product of plasmon-driven reduction of 4-NBT on AuMPs. Moreover, recently reported results suggest that the rates of hot carrier-driven reactions can be controlled by the electric field which in turn can be altered by the intensity of the laser light.[38] These findings are in good agreement with the results reported by the Jain[52,53] and Schultz[54,55] groups which shows that the intensity of laser light can be used to control the selectivity of catalytic reactions on plasmonic nanostructures.

Using gas chromatography coupled to mass spectroscopy (GC-MS), we previously demonstrated that Au@PdMPs are capable of catalyzing the Suzuki–Miyaura coupling reaction between 4-bromobenzenethiol and 4-mercaptophenylboronic acid (4-MPBA).[39] In that experiment, Au@PdMPs with a monolayer of 4-bromobenzenethiol (4-BrBT) were exposed to a solution of 4-MPBA and electromagnetic radiation. The Suzuki–Miyaura coupling reaction yielded biphenyldithiol (BPDT) that was detected using GC-MS and TERS. We also found that molecular analytes on Au@PdMP surfaces are oriented nearly planarly (10–12°) relative to the metal surface, which facilitates a coupling reaction that takes place on their surfaces.[36]

Expanding on this discovery, we investigate the extent to which TERS can be used to probe the molecular reactivity in bimolecular plasmon-driven reactions. For this, we deposit one reactant on the sample of interest, whereas the second reactant is deposited on the scanning probe. Next, we bring the probe on the sample surface and illuminate it with continuous wavelength laser light. This catalyzes the reaction between two analytes. In this study, we show that this modified TERS approach named cargo-TERS can be used for *in situ* elucidation of the reactivity of three aromatic halides, 4-bromo-, 4-chloro- and 4-fluoro-thiophenols (4-BTP, 4-CTP and 4-FTP) in the Suzuki–Miyaura coupling reaction with 4-MPBA. Our findings show that cargo-TERS can be used for highly accurate assessment of the molecular reactivity of these analytes requiring femto or attoliters of analytes.

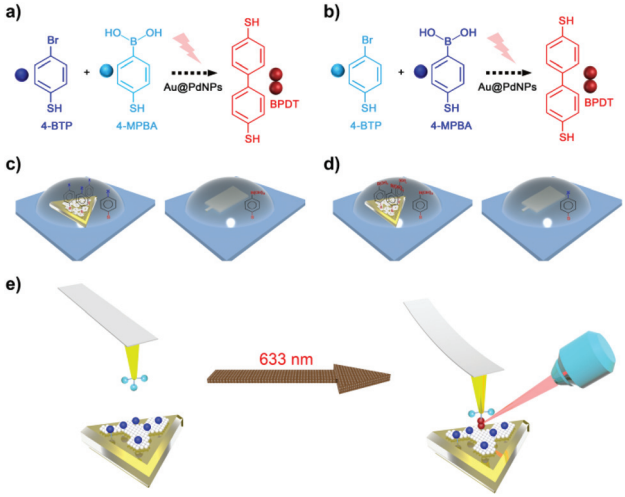

Scheme 1 Illustration of cargo-TERS experiments on Au@PdNPs. (a and b) A schematic representation of the Suzuki–Miyaura coupling reaction between 4-XTP and 4-MPBA, where X = Br, Cl or F. (c) Modification of Au@PdNPs with 4-XTP and Au-coated scanning probes with 4-MPBA. (d) Modification of Au@PdNPs with 4-MPBA and Au-coated scanning probes with 4-XTP. (e) Plasmon-driven Suzuki–Miyaura coupling of 4-MPBA and 4-XTP on the surface of Au@PdNPs that yields BPDT.

Results and discussion

For monitoring the process before and after the reaction, we use TERS to measure the Raman spectral change. For TERS, firstly we coated Au@PdNPs with a monolayer of 4-XTP (X = F, Cl and Br) to investigate the intrinsic vibrational signal of the halogen–benzene on the surface of the bimetallic nanostructures (Scheme 1) before the reaction. Au@PdNPs were prepared using a three-step synthetic approach, Fig. S1.† Briefly, seed-mediated growth of 15 nm thin AuNPs (Fig. S2†) was followed by the isotropic growth of these nanoplates to reach 70 nm-thick AuNPs (Fig. S3†) that were exposed to Pd ions to fabricate Au@PdNPs. These bimetallic nanostructures had a sub-monolayer of Pd on their surface (Fig. S4†). Au@PdNPs used in this work had around 200–300 nm width and ~70 nm height (see the SEM image in Fig. S5†). We first deposited 4-BTP on the surface of these nanoplates (Scheme 1c). TERS spectra of 4-BTP showed two distinct vibrational bands at 1064 and 1556 cm^{-1} that corresponded to the vibration modes of the benzene ring (Fig. 1a, traces 1 and 2, more TERS spectra can be seen in Fig. S6†).[56] TERS images of Au@PdNPs with an unmodified Au-coated tip confirmed the presence of 4-BTP on the surface of Au@PdNPs (Fig. S7†). Next, we deposited 4-MPBA on the Au-coated scanning probe (Scheme 1c and Fig. 1b, traces 5 and 6). The spectrum of 4-MPBA had two vibrational bands at 1070 and 1585 cm^{-1} that allowed for unambiguous identification of this molecular analyte. Finally, we imaged the surface of 4-BTP-modified Au@PdNPs using the 4-MPBA-modified Au-coated scanning probe, Scheme 1a and e and Fig. 1d–h. This triggered the Suzuki–Miyaura coupling reaction between two molecular analytes yielding BPDT. The reaction product exhibits a vibrational band at 1593 cm^{-1} (Fig. 1c, traces 9 and 10 and Fig. S8†), which allows for its detection on Au@PdNPs.

Our results also show that cargo-TERS can be used for the quantification of BPDT catalytic probability (Fig. 1g and h) on Au@PdNPs. For this, one has to count the spectra that show the presence of the reaction product (1593 cm^{-1}) in the acquired TERS maps of bimetallic nanostructures. If the sizes of the nanostructures are similar or identical and TERS images were obtained with the same spatial resolution, the catalytic probability of the reaction product can be directly reported. However, if the size of Au@PdNPs had substantial variability or different spatial resolutions were used upon their TERS imaging, the total number of spectra that contain 1593 cm^{-1}

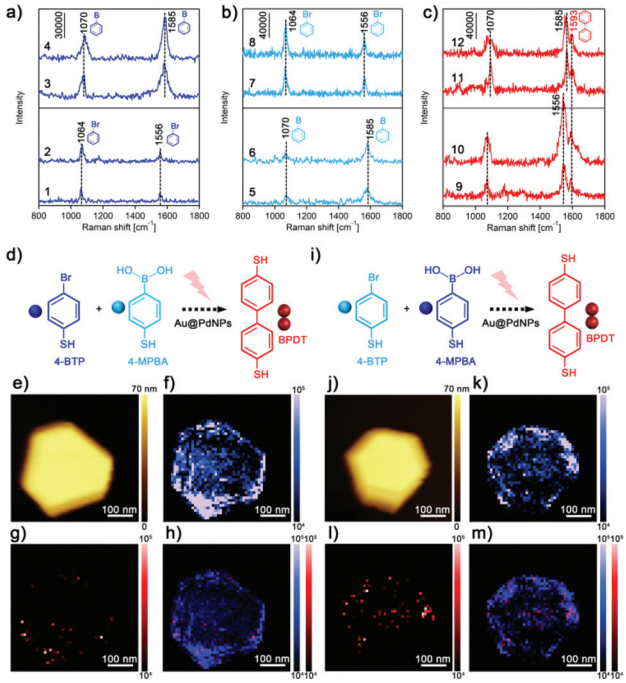

Fig. 1 (a) Representative TERS spectra of 4-BTP (1,2) and 4-MPBA (3,4) on the surface of Au@PdNPs; (b) surface-enhanced Raman spectra (SERS) of 4-MPBA (5,6) and 4-BTP (7,8) on a Au-coated probe. (c) TERS spectra of BPDT on Au@PdNPs. (d) The schematic representation of the Suzuki–Miyaura coupling reaction between 4-BTP-modified Au@PdNPs and the 4-MPBA-modified Au-coated probe; (e) AFM and the corresponding (f) TERS image of 4-BTP-modified Au@PdNPs before the Suzuki–Miyaura coupling reaction and (g) after demonstrating the formation of BPDT (red pixels). (h) An overlay TERS image of 4-BTP (blue) and BPDT (red) signals on Au@PdNPs. (i) The schematic representation of the Suzuki–Miyaura coupling reaction between the 4-BTP-modified Au-coated probe and 4-MPBA-modified Au@PdNPs. (j) AFM and the corresponding (k) TERS image of 4-MPBA-modified Au@PdNPs before the Suzuki–Miyaura coupling reaction and (l) after demonstrating the formation of BPDT (red pixels). (m) An overlay TERS image of 4-MPBA (blue) and BPDT (red) signals on Au@PdNPs. The scale bar in each image is 100 nm.

can be divided over the total number of collected spectra from a nanostructure. This approach, as discussed below, allows for direct comparison of the molecular reactivity of aromatic halides in plasmon-driven reactions.

It is important to demonstrate that the catalytic probability of such a coupling reaction is independent of the localization of molecular analytes between the probe and the sample. In the parallel experiment, we deposited 4-MPBA on the surface of Au@PdNPs and 4-BTP on the Au-coated scanning probe (Scheme 1b and d). Next, we performed cargo-TERS to investigate the catalytic probability of BPDT formed on the surface of Au@PdNPs (Fig. 1i–m). The same as in the initial experiment, we detected a new band at 1593 cm^{-1}, which indicated the formation of BPDT (Fig. 1c, traces 11 and 12). We also found that an opposite to the initial experiment arrangement of molecular analytes yielded a similar amount of BPDT (discussed below) on the surface of the bimetallic nanostructures. It should be noted that when only one molecular analyte was present on the scanning probe of Au@PdNPs, no BPDT products were observed (Fig. S7†).

Next, we examined the molecular reactivity of 4-CTP and 4-FTP in the Suzuki–Miyaura coupling reaction on Au@PdNPs. The TERS spectra of 4-CTP exhibited three distinct vibrational bands at 1069, 1098 and 1567 cm^{-1} (Fig. 2d),[57] whereas two bands were detected in the spectrum of 4-FTP at 1076 and 1577 cm^{-1} (Fig. 2a). Prior to cargo-TERS, we first confirmed the presence of 4-CTP and 4-FTP on the surface of Au@PdNPs using unmodified scanning probes. In both cases, we observed the full surface coverage of the reactants on Au@PdNPs (Fig. S9 and S10†). Cargo-TERS with the 4-MPBA-modified Au-coated scanning probe (Fig. 2b and e) revealed the formation of BPDT (Fig. 2c, f and 3a-I, see more TERS spectra of BPDT in Fig. S11†). We found that 4-CTP resulted in a substantially lower catalytic probability of BPDT (3.52%) compared to the

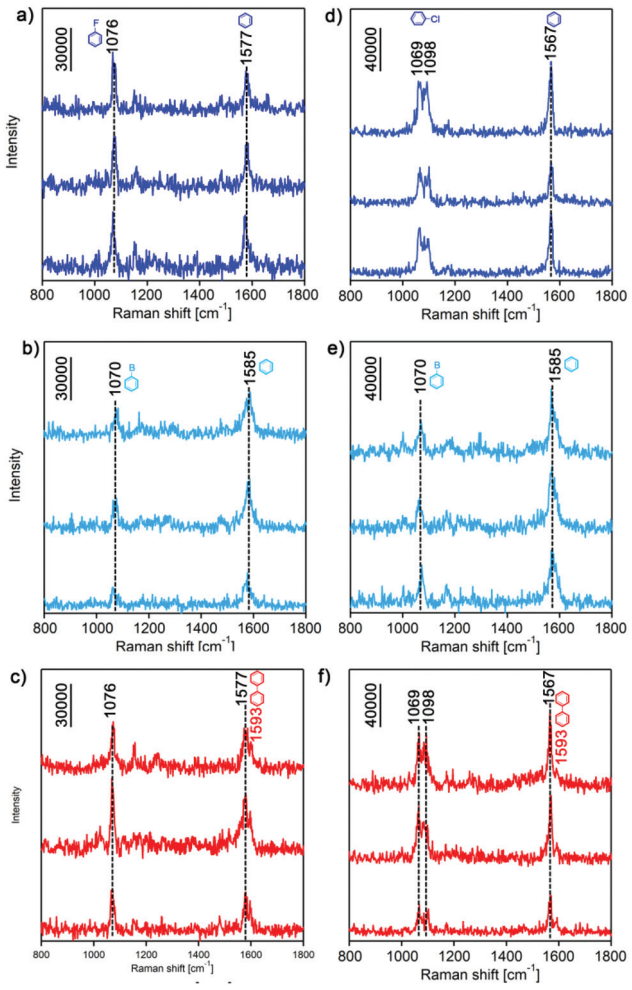

Fig. 2 (a) Representative TERS spectra of 4-FTP, (b) SERS spectra of 4-MPBA and (c) BPDT formed on Au@PdNPs was a result of the Suzuki–Miyaura coupling reaction between 4-FTP and 4-MPBA. (d) Representative TERS spectra of 4-CTP, (e) SERS spectra of 4-MPBA and (f) BPDT formed on Au@PdNPs was a result of the Suzuki–Miyaura coupling reaction between 4-CTP and 4-MPBA.

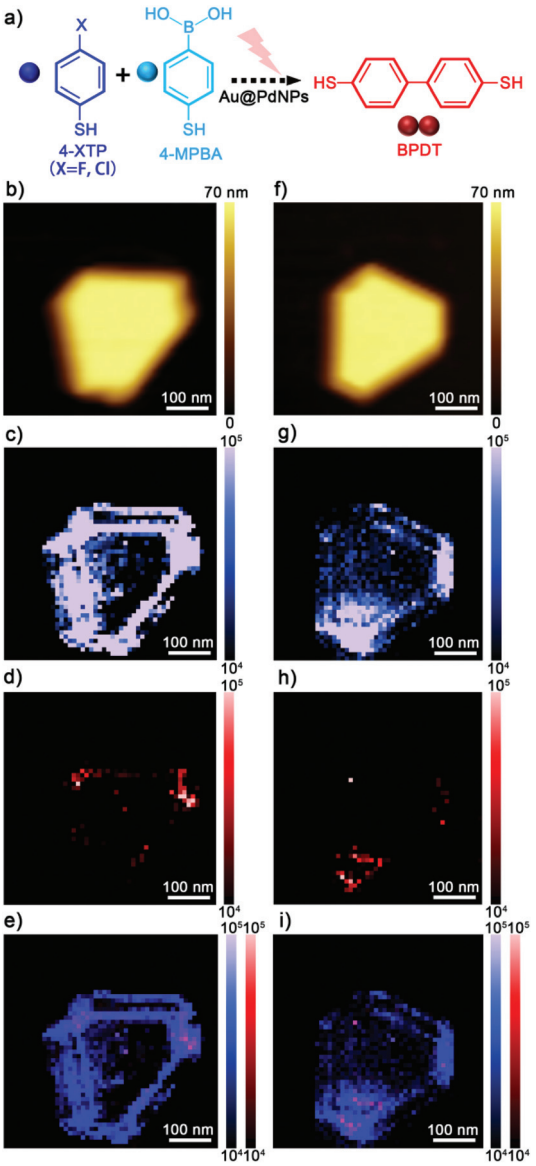

Fig. 3 (a) The schematic representation of the Suzuki–Miyaura coupling reaction between the 4-XTP-modified Au-coated (X = Cl and F) probe and 4-MPBA-modified Au@PdNPs. (b) AFM and the corresponding (c) TERS image of 4-CTP-modified Au@PdNPs before the Suzuki–Miyaura coupling reaction and (d) after demonstrating the formation of BPDT (red pixels). (e) An overlay TERS image of 4-CTP (blue) and BPDT (red) signals on Au@PdNPs. (f) AFM and the corresponding (g) TERS image of 4-FTP-modified Au@PdNPs before the Suzuki–Miyaura coupling reaction and (h) after demonstrating the formation of BPDT (red pixels). (i) An overlay TERS image of 4-FTP (blue) and BPDT (red) signals on Au@PdNPs.

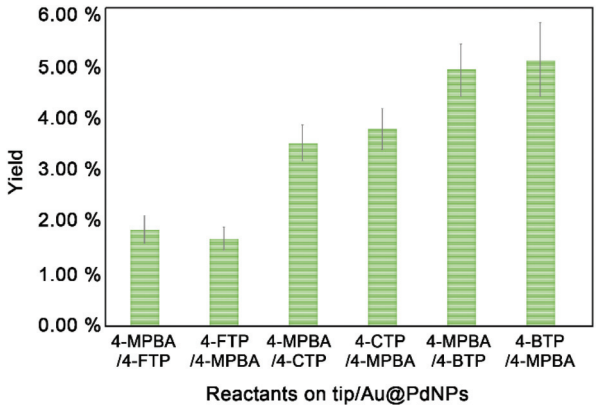

Fig. 4 The catalytic probability of BPDT in six different cargo-TERS experiments. The catalytic probability of BPDT was obtained by counting the number of spectra that exhibited a 1593 cm^{-1} band with regard to the total number of TERS spectra acquired. At least three individual Au@PdNPs were analyzed in each of the reported experiments. Average catalytic probability observed in all the Au@PdNPs is reported with the corresponding standard deviations.

catalytic probability of the coupling reaction between 4-BTP and 4-MPBA (4.94%), Fig. 4 and Table S1.† These results are in good agreement with the previously reported GC-MS findings. Li and co-workers found that the Suzuki–Miyaura coupling reaction between 4-BTP and 4-MPBA on Au@PdMPs catalyzed only micromoles of BPDT.[39] We also found that the use of 4-FTP as an aromatic halide catalyzed even fewer BPDT (1.87%) on the surface of Au@PdNPs that were observed with the use of 4-CTP. To determine the catalytic probability of BPDT, we counted the number of TERS spectra that exhibited a 1593 cm^{-1} band, which unambiguously confirmed the presence of BPDT on the Au@PdNP surface. Next, we divided this number by the total number of spectra collected from the surface of Au@PdNPs. It should be noted that the sizes of these bimetallic nanostructures were nearly identical in all these experiments, as well as the spatial resolution used in TERS imaging on their surfaces. We also analyzed at least three individual bimetallic nanostructures to determine the standard deviations of the reported catalytic probability of BPDT in our experiments (Fig. 4). Our results suggest that cargo-TERS allows for an elucidation of the reactivity of aromatic halides on Au@PdNPs with high accuracy.

One may wonder if the catalytic probability of the Suzuki–Miyaura coupling reaction between 4-MPBA and the analyzed aromatic halides (4-CTP and 4-FTP) is independent of the reactant localization in cargo-TERS. To answer this question, we investigated the catalytic probability of BPDT with 4-CTP- and 4-FTP-modified Au-probes and 4-MPBA-coated Au@PdNPs. We found that the catalytic probability of the reaction is independent of the localization of halides and boronic acid derivatives between the probe and the sample. It should also be noted that in the absence of 4-MPBA, no reaction product was detected with either 4-CTP or 4-FTP present on the tip or the sample surface. It is also important to demonstrate that the catalytic probability of BPDT does not depend on the number of cargo-TERS scans. By other means, if Au@PdNPs will be scanned again with the same modified probe, the catalytic probability of BPDT would not be changed. To demonstrate this, we carried out the second round of cargo-TERS on the 4-CTP modified Au@PdNPs which were already analyzed using a 4-MPBA modified probe. We found no significant changes in

the catalytic probability of BPDT between the first (Fig. S12a–d†) and second rounds (Fig. S12e–h†) of cargo-TERS imaging. This experiment demonstrated that the catalytic probability of BPDT cannot be altered by additional cargo-TERS imaging which demonstrates the high robustness of this analytical approach.

Cargo-TERS with less reactive 4-CTP and 4-FTP also showed that the edges and corners of Au@PdNPs exhibited higher reactivity than the terraces located in the central part of these bimetallic nanostructures (Fig. 1g, h, l, m and 3a–i). Such an enhanced catalytic reactivity of edges and corners was reported by several research groups.[37,41,49] Using DFT calculations, the Ren's group examined the electronic density of states (DOS) of d-bands on the Pd atom located at the step edge and compared them with the DOS of d-bands on the Pd atoms on terraces. Zhong and co-workers found that the DOS of the step-edge Pd atom had a global shift to higher energy simultaneously exhibiting narrowing of the d-band, as a result of its unsaturated coordination. This resulted in a decrease in inter-atom coupling. These calculations also revealed the coupling between the σ-bonds of the analytes and d-bands on Pd. It was found that the σ orbitals of the analyte adsorbed at the step edge were at higher energies compared to the σ orbitals of analytes at the terrace, indicating a weaker σ–d interaction at the step edge. Our findings show that the edge-facilitated reactivity is insignificant for highly reactive analytes, such as 4-BTP. However, this effect becomes prevalent for plasmon-driven reactions between reactants with weaker reactivity.

These findings further extend the frontiers of the innovative concept of chemically-modified scanning probe TERS, which was first introduced by the Apkarian group. Specifically, Lee and co-workers[58] showed that carbon monoxide at the apex of the scanning probe can be used as a rectifying plasmonic nanoantenna allowing for Angstrom spatial resolution in TERS imaging. Recently, Crampton and co-workers demonstrated that localization of cobalt tetraphenylporphyrin (CoTPP) on the TERS scanning probe[59] allows for the phase determination of intramolecular currents and the polarity control of the nonlinear diode-like optoelectronic response in TERS imaging. Our work showed that such chemically-modified scanning probe TERS, named by us cargo-TERS, can be used to determine the molecular reactivity *via* examination of the catalytic probability of the corresponding reaction product.

Just as any analytical approach, cargo-TERS is likely to have some limitations that should be investigated and resolved in future studies. At the first glance, one can expect that cargo-TERS may be limited to the determination of the catalytic probability of only plasmon-driven processes. Although more work is required to address this concern, we expect that TERS in general and cargo-TERS in particular can be broadly used to probe reactions that lead to chemical transformations detectable through alteration of the vibrational fingerprints of either analytes or the reaction products. The applicability of TERS in such cases is likely to be determined by a match between the TERS response and the reaction timescale. Therefore, the development of femto and pico-second resolution in TERS (the timescale on which most of the reactions are taking place) is strongly desired. It should also be noted that the analyzed molecules in cargo-TERS ought to have thiol bonds to enable their anchoring to the metallic surfaces. Although this is not required for the examination of the molecular reactivity, thiol bonds allow for chemisorption of analytes and the corresponding products to metallized surfaces minimizing unpreferred contamination of scanning probes used in TERS. One can expect that such chemisorption can be substituted by molecular physisorption that can be achieved at low temperatures (low temperature TERS).[15] In this case, the use of thiols may be avoided to examine the molecular reactivity in real time.

Conclusions

Our findings demonstrate that cargo-TERS can be used for fast, robust and reliable analysis of molecular reactivity plasmon-driven reactions. Using this approach, we were able to probe the reactivity of aromatic halides in a plasmon-driven Suzuki–Miyaura coupling reaction. We also showed that cargo-TERS can be used to probe the nanoscale reactivity of bimetallic catalysts unraveling sites with high and low reactivity. This approach requires a single monolayer of reactants and can be performed within seconds to reveal the reactivity of molecular analytes. This analytical approach can be used to tailor the design of molecular reactants and catalysts for desired reactivity and catalytic properties, ultimately leading to highly efficient, selective and green catalysis. These findings open up a new avenue for the direct analysis of molecular interactions that in turn can be used for the prediction of the biological activity of novel classes of drugs candidates and the selectivity of chemical catalysts. In addition, the coupling between different molecules by this method is highly useful for achieving other reactions such as the Heck reaction[60] in plasmon-driven polymerizations.[61]

Author contributions

Z. L. carried out the synthetic experiments; D. K. and Z. L. analysed the experimental data; Z. L. carried out the SEM analyses; D. K. and Z. L. conceived the central idea, coordinated the work, and analysed the experimental data. D. K. and Z. L. wrote the manuscript.

Conflicts of interest

There are no conflicts to declare.

Acknowledgements

We are grateful to AgriLife Research of Texas A&M for the financial support. We also acknowledge Governor's University Research Initiative (GURI) grant program of Texas A&M University, GURI Grant Agreement No. 12-2016, M1700437.

Notes and references

1 H. Ren, S. Yu, L. Chao, Y. Xia, Y. Sun, S. Zuo, F. Li, T. Niu, Y. Yang and H. Ju, *Nat. Photonics*, 2020, **14**, 154–163.
2 J. Chung, A. M. Kushner, A. C. Weisman and Z. Guan, *Nat. Mater.*, 2014, **13**, 1055–1062.
3 S. Laschat, A. Baro, N. Steinke, F. Giesselmann, C. Haegele, G. Scalia, R. Judele, E. Kapatsina, S. Sauer and A. Schreivogel, *Angew. Chem., Int. Ed.*, 2007, **46**, 4832–4887.
4 S. Keten, Z. Xu, B. Ihle and M. Buehler, *Nat. Mater.*, 2010, **9**, 359–367.
5 M. A. Czarnecki, Y. Morisawa, Y. Futami and Y. Ozaki, *Chem. Rev.*, 2015, **115**, 9707–9744.
6 G. Townshend, G. S. Thompson, L. J. White, J. R. Hiscock and J. L. Ortega-Roldan, *Chem. Commun.*, 2020, **56**, 4015–4018.
7 D. Kurouski, A. Dazzi, R. Zenobi and A. Centrone, *Chem. Soc. Rev.*, 2020, **39**, 3315–3347.
8 P. Verma, *Chem. Rev.*, 2017, **117**, 6447–6466.
9 T. X. Huang, S. C. Huang, M. H. Li, Z. C. Zeng, X. Wang and B. Ren, *Anal. Bioanal. Chem.*, 2015, **407**, 8177–8195.
10 T. Deckert-Gaudig, A. Taguchi, S. Kawata and V. Deckert, *Chem. Soc. Rev.*, 2017, **46**, 4077–4110.
11 M. Moskovits, *J. Chem. Phys.*, 1978, **69**, 4159–4161.
12 F. W. King, R. P. Van Duyne and G. C. Schatz, *J. Chem. Phys.*, 1978, **69**, 4472–4481.
13 S. L. Kleinman, B. Sharma, M. G. Blaber, A. I. Henry, N. Valley, R. G. Freeman, M. J. Natan, G. C. Schatz and R. P. Van Duyne, *J. Am. Chem. Soc.*, 2013, **135**, 301–308.
14 K. L. Wustholz, A.-I. Henry, J. M. McMahon, R. G. Freeman, N. Valley, M. E. Piotti, M. J. Natan, G. C. Schatz and R. P. Van Duyne, *J. Am. Chem. Soc.*, 2010, **132**, 10903–10910.
15 R. Zhang, Y. Zhang, Z. Dong, S. Jiang, C. Zhang, L. Chen, L. Zhang, Y. Liao, J. Aizpurua, Y. Luo, J. L. Yang and J. G. Hou, *Nature*, 2013, **498**, 82–86.
16 M. D. Sonntag, J. M. Klingsporn, L. K. Garibay, J. M. Roberts, J. A. Dieringer, T. Seideman, K. A. Scheidt, L. Jensen, G. C. Schatz and R. P. Van Duyne, *J. Phys. Chem. C*, 2012, **116**, 478–483.
17 J. Lee, K. T. Crampton, N. Tallarida and V. A. Apkarian, *Nature*, 2019, **568**, 78–82.
18 Z. He, Z. Han, M. Kizer, R. J. Linhardt, X. Wang, A. M. Sinyukov, J. Wang, V. Deckert, A. V. Sokolov, J. Hu and M. O. Scully, *J. Am. Chem. Soc.*, 2018, **141**, 753–757.
19 R. Treffer and V. Deckert, *Curr. Opin. Biotechnol.*, 2010, **21**, 4–11.
20 A. V. Krasnoslobodtsev, T. Deckert-Gaudig, Y. Zhang, V. Deckert and Y. L. Lyubchenko, *Ultramicroscopy*, 2016, **165**, 26–33.
21 D. Kurouski, T. Deckert-Gaudig, V. Deckert and I. K. Lednev, *J. Am. Chem. Soc.*, 2012, **134**, 13323–13329.
22 D. Kurouski, T. Deckert-Gaudig, V. Deckert and I. K. Lednev, *Biophys. J.*, 2014, **106**, 263–271.
23 S. Bonhommeau, D. Talaga, J. Hunel, C. Cullin and S. Lecomte, *Angew. Chem., Int. Ed.*, 2017, **56**, 1771–1774.
24 S. Henry, N. B. Bercu, C. Bobo, C. Cullin, M. Molinari and S. Lecomte, *Nanoscale*, 2018, **10**, 936–940.
25 E. Lipiec, D. Perez-Guaita, J. Kaderli, B. R. Wood and R. Zenobi, *Angew. Chem., Int. Ed.*, 2018, **130**, 8655–8660.
26 W. Su, N. Kumar, A. Krayev and M. Chaigneau, *Nat. Commun.*, 2018, **9**, 2891.
27 S. Mahapatra, J. F. Schultz, Y. Ning, J. L. Zhang and N. Jiang, *Nanoscale*, 2019, **11**, 19877–19883.
28 A. G. Milekhin, M. Rahaman, E. E. Rodyakina, A. V. Latyshev, V. M. Dzhagan and D. R. T. Zahn, *Nanoscale*, 2018, **10**, 2755–2763.
29 J. H. Park, G. von Maltzahn, L. L. Ong, A. Centrone, T. A. Hatton, E. Ruoslahti, S. N. Bhatia and M. J. Sailor, *Adv. Mater.*, 2010, **22**, 880–885.
30 W. Dai, F. Shao, J. Szczerbiński, R. McCaffrey, R. Zenobi, Y. Jin, A. D. Schlüter and W. Zhang, *Angew. Chem., Int. Ed.*, 2016, **128**, 221–225.
31 L. Q. Zheng, X. Wang, F. Shao, M. Hegner and R. Zenobi, *Angew. Chem., Int. Ed.*, 2018, **57**, 1025–1029.
32 N. Martin Sabanes, T. Ohto, D. Andrienko, Y. Nagata and K. F. Domke, *Angew. Chem., Int. Ed.*, 2017, **56**, 9796–9801.
33 Z. C. Zeng, S. C. Huang, D. Y. Wu, L. Y. Meng, M. H. Li, T. X. Huang, J. H. Zhong, X. Wang, Z. L. Yang and B. Ren, *J. Am. Chem. Soc.*, 2015, **137**, 11928–11931.
34 D. Kurouski, M. Mattei and R. P. Van Duyne, *Nano Lett.*, 2015, **15**, 7956–7962.
35 T. Touzalin, S. Joiret, I. T. Lucas and E. Maisonhaute, *Electrochem. Commun.*, 2019, **108**, 106557.
36 Z. Li, P. El-Khoury and D. Kurouski, *Chem. Commun.*, 2021, (57), 891–894.
37 Z. Li and D. Kurouski, *J. Phys. Chem. C*, 2020, **124**, 12850–12854.
38 Z. Li, J. Rigor, N. Large, P. El-Khoury and D. Kurouski, *J. Phys. Chem. C*, 2021, **125**, 2492–2501.
39 Z. Li, R. Wang and D. Kurouski, *J. Phys. Chem. Lett.*, 2020, **11**, 5531–5537.
40 E. M. van Schrojenstein Lantman, T. Deckert-Gaudig, A. J. Mank, V. Deckert and B. M. Weckhuysen, *Nat. Nanotechnol.*, 2012, **7**, 583–586.
41 C. F. Wang, B. T. O'Callahan, D. Kurouski, A. Krayev and P. Z. El-Khoury, *J. Phys. Chem. Lett.*, 2020, **11**, 3809–3814.
42 C. F. Wang, B. T. O'Callahan, D. Kurouski, A. Krayev, Z. D. Schultz and P. Z. El-Khoury, *J. Phys. Chem. Lett.*, 2020, **11**, 5890–5895.
43 R. Wang, J. Li, J. Rigor, N. Large, P. El-Khoury, R. A. Yu and D. Kurouski, *J. Phys. Chem. C*, 2020, **124**, 2238–2244.
44 M. L. Brongersma, N. J. Halas and P. Nordlander, *Nat. Nanotechnol.*, 2015, **10**, 25–34.
45 A. Manjavacas, J. G. Liu, V. Kulkarni and P. Nordlander, *ACS Nano*, 2014, **8**, 7630–7638.
46 L. Zhou, J. M. P. Martirez, J. Finzel, C. Zhang, D. F. Swearer, S. Tian, H. Robatjazi, M. Lou, L. Dong, L. Henderson, P. Christopher, E. A. Carter, P. Nordlander and N. J. Halas, *Nat. Energy*, 2020, **5**, 61–70.
47 A. M. Brown, R. Sundararaman, P. Narang, W. A. Goddard III and H. A. Atwater, *ACS Nano*, 2015, **10**, 957–966.

48 P. Narang, R. Sundararaman and H. A. Atwater, *Nanophotonics*, 2016, **5**, 96–111.
49 J. H. Zhong, X. Jin, L. Meng, X. Wang, H. S. Su, Z. L. Yang, C. T. Williams and B. Ren, *Nat. Nanotechnol.*, 2017, **12**, 132–136.
50 A. Bhattarai, K. T. Crampton, A. G. Joly, L. Kovarik, W. P. Hess and P. Z. El-Khoury, *J. Phys. Chem. Lett.*, 2018, **9**, 7105–7109.
51 A. Bhattarai, I. V. Novikova and P. Z. El-Khoury, *J. Phys. Chem. C*, 2019, **123**, 27765–27769.
52 S. Yu and P. K. Jain, *Angew. Chem.*, 2020, **59**, 2085–2088.
53 S. Yu, A. J. Wilson, J. Heo and P. K. Jain, *Nano Lett.*, 2018, **18**, 2189–2194.
54 L. Xiao and Z. D. Schultz, *Anal. Chem.*, 2018, **90**, 440–458.
55 D. A. Nelson and Z. D. Schultz, *J. Phys. Chem. C*, 2018, **122**, 8581–8588.
56 Y. Zhao, L. Du, H. Li, W. Xie and J. Chen, *J. Phys. Chem. Lett.*, 2019, **10**, 1286–1291.
57 P. Jiang, Y. Dong, L. Yang, Y. Zhao and W. Xie, *J. Phys. Chem. C*, 2019, **123**, 16741–16746.
58 J. Lee, N. Tallarida, X. Chen, L. Jensen and V. A. Apkarian, *Sci. Adv.*, 2018, **4**, eaat5472.
59 K. T. Crampton, J. Lee and V. A. Apkarian, *ACS Nano*, 2019, **13**, 6363–6371.
60 Z. Zhang, C. R. Rogers and E. A. Weiss, *J. Am. Chem. Soc.*, 2019, **142**, 495–501.
61 K. Ueno, S. Juodkazis, T. Shibuya, Y. Yokota, V. Mizeikis, K. Sasaki and H. Misawa, *J. Am. Chem. Soc.*, 2008, **130**, 6928–6929.